Journal of *Marine Science and Engineering*

MDPI

Article

Derivation of the Controllable Region for Attitude Control of Towfish and Verification Through Water Tank Test

Jihyeong Lee [1] and Min-Kyu Kim [2,*]

[1] Maritime ICT & Mobility Research Department, Korea Institute of Ocean Science & Technology, Busan 49111, Republic of Korea; wlgud0818@kiost.ac.kr
[2] Maritime Robotics Test & Evaluation Center, Korea Institute of Ocean Science & Technology, Pohang 37553, Republic of Korea
* Correspondence: kmk7059@kiost.ac.kr; Tel.: +82-54-240-3506

Abstract: We investigated the attitude control of a towfish to enhance the image quality of its sound navigation ranging system. The target towfish is equipped with two elevators on the horizontal tail wing, and attitude control is performed using these actuators. In particular, when a high-resolution sonar system is mounted on the towfish, any irregular movement can cause defocusing; thus, attitude control of the towfish is essential. Because the towfish has no thrust of its own and moves by being connected to a mother vessel via a cable, its attitude must be controlled by comprehensively analyzing its towing force and equation of motion. Herein, we propose a method for calculating the region where the attitude of the towfish can be controlled based on changes in the center of gravity, towing speed, and towing point. We conducted a water tank test to verify this method and confirmed that the attitude of the towfish could be controlled in controllable areas but not in uncontrollable regions.

Keywords: towfish; elevator; controllable region; attitude control; towing point

check for updates

Academic Editor: Lúcia Moreira

Received: 24 March 2025
Revised: 16 April 2025
Accepted: 21 April 2025
Published: 23 April 2025

Citation: Lee, J.; Kim, M.-K. Derivation of the Controllable Region for Attitude Control of Towfish and Verification Through Water Tank Test. *J. Mar. Sci. Eng.* **2025**, *13*, 834. https://doi.org/10.3390/jmse13050834

Copyright: © 2025 by the authors. Licensee MDPI, Basel, Switzerland. This article is an open access article distributed under the terms and conditions of the Creative Commons Attribution (CC BY) license (https://creativecommons.org/licenses/by/4.0/).

1. Introduction

Typically, a towfish does not have its own thrust device and is maneuvered using a connected cable with the mother vessel [1]. This limits the movement of the towfish but enables long-term and wide-area observations because it can be continuously supplied with power from the mother ship [2,3]. Recently, there has been an increase in the demand for underwater surveillance, reconnaissance, and exploration of seabed resources in the civil and defense sectors. Consequently, various sound navigation ranging (sonar) have been developed and applied to meet this demand [4–6].

A towfish is shaped like a long cylinder to enable hydrodynamically stable movement. However, when the attitude is not continuously controlled, towfish cannot respond to unpredictable sea or underwater environments. This is particularly critical for mounting high-resolution sonar systems on the towfish, such as interferometric synthetic aperture sonar (InSAS). In this case, any abnormal motion of the towfish defocuses the InSAS image [7,8]. Therefore, to improve image quality, a function that can precisely control the attitude of towfish in real time is required [9–11].

This study aims to establish criteria for easily selecting the towing point by calculating the region where the attitude of the towfish can be controlled. Although research on towfish is actively being conducted and applied in various fields, studies with a purpose similar to this study are scarce. Most studies on towfish focus on simply controlling them. Studies on attitude, turn maneuvering, and depth control [12–18], as well as route generation to avoid

obstacles [19,20], have been conducted. In addition, studies have determined the hydrodynamic derivative of towfish using computational fluid dynamics [2,21] analysis, whereas other works have analyzed the motion characteristics of towfish systems through modeling and simulation. However, these related studies simply focus on one goal, such as towfish control, analysis, and modeling. Previous studies related to this study include [22,23]. However, these studies simply presented the controllable towing point region through simulations and did not verify the results through actual water tank tests.

To derive the towing point for easy attitude control, six-degree-of-freedom (6-DOF) equations of motion for the towfish are derived. Subsequently, the dynamic relationship between the towing point and the 6-DOF equations of motion is analyzed. Particularly, for attitude control using an elevator, an analysis considering the relationship with the actuator capacity is required. In addition, considering the towing speed of the towfish, the controllable region of a towing point where the attitude of the towfish can be easily controlled is presented.

This study deals with the method of calculating the region of controllable towing point for the purpose of making the attitude control of towfish easier. And it was verified through a water tank test that the region of the towing point was calculated correctly. These research results will provide an opportunity to select the towing point correctly when operating a towfish. In addition, it can be used as an indicator for selecting the location of the center of gravity and center of buoyancy during the design and manufacturing stage of a towfish.

2. Target Towfish and Actuator

Figure 1a,b show the target towfish and actuator, respectively. The towfish is connected to the towing point with a cable (Figure 1a). For attitude control, the pitch and roll of the towfish are controlled using elevators. Because the towfish cannot receive position information from a global positioning system, position was obtained using an ultra-short baseline (USBL) instead, and the attitude was obtained using an inertial measurement unit (IMU). The selected elevator wing shape was NACA0018, which was provided by the National Advisory Committee for Aeronautics (NACA). The specifications of the towfish are presented in Table 1.

Table 1. Specifications of the towfish.

Towfish			
Length	3.5 m	Weight in air	2940 N
Diameter	0.4 m	Buoyancy	490 N
Towing speed	$\leq$2 m/s	Towing speed	$\leq$2 m/s
Single elevator area	0.025 m^2		
Sensor (Manufacturer/Model)		**Performance**	
IMU (Advanced Navigation/Spatial FOG Dual)		0.01° pitch, roll and heading 0.05°/HR FOG Gyro	
USBL (Advanced Navigation/Subsonus)		0.1 m position accuracy 1000 m depth and range	



Figure 1. Target towfish (**a**) and actuator (**b**).

3. Dynamic Equations of Motion for the Towfish

3.1. Coordinate System

To analyze the motion of the towfish, a coordinate system is introduced (Figure 2). A body-fixed coordinate system is fitted with the center of the body of the towfish, whereas an earth-fixed coordinate system is fitted with the center of the earth. The body-fixed coordinate system was used to analyze the motion of the towfish, whereas the earth-fixed coordinate system was used to analyze the position and angle of the towfish.

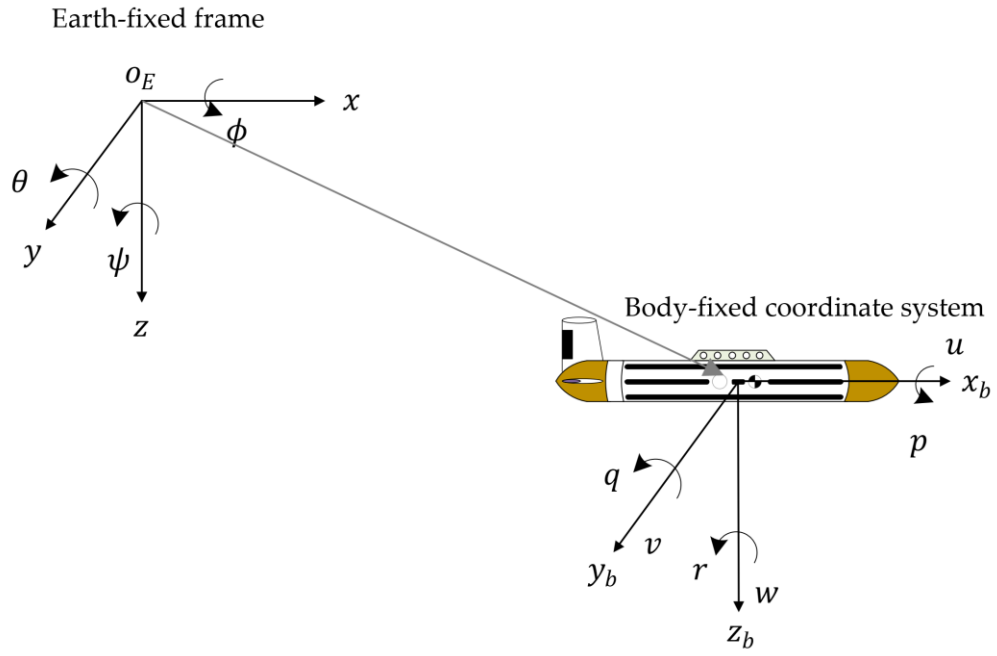


Figure 2. Earth- and body-fixed coordinate systems.

The earth-fixed coordinate system O_E comprises $(x, y, z, \phi, \theta, \psi)$, where (x, y, z) is the position of the towfish and (ϕ, θ, ψ) represents the roll, pitch, and yaw angles of a towfish. The body-fixed coordinate system $x_b y_b z_b$ comprises (u, v, w, p, q, r), where (u, v, w) and (p, q, r) are the linear and angular velocities in three axes, respectively.

The motion characteristics of the towfish can be analyzed by converting the body-fixed coordinate system to the earth-fixed coordinate system. Herein, the linear and angular velocities of the towfish were converted to the position and Euler angles of the earth-fixed coordinate system using Equation (1) [22].

$$\dot{\eta} = J(\eta_2)\nu, \tag{1}$$

$$J(\boldsymbol{\eta}_2) = \begin{pmatrix} J_1(\boldsymbol{\eta}_2) & 0_{3\times3} \\ 0_{3\times3} & J_2(\boldsymbol{\eta}_2) \end{pmatrix}, \tag{2}$$

$$J_1(\boldsymbol{\eta}_2) = \begin{pmatrix} c\psi c\theta & -s\psi c\psi + c\psi s\theta s\phi & s\psi s\phi + c\psi c\phi s\theta \\ s\psi c\theta & c\psi c\phi + s\phi s\theta s\psi & -c\psi s\phi + s\theta s\psi c\phi \\ -s\theta & c\theta s\phi & c\theta c\phi \end{pmatrix}, \tag{3}$$

$$J_2(\boldsymbol{\eta}_2) = \begin{pmatrix} 1 & s\phi t\theta & c\phi t\theta \\ 0 & c\phi & -s\phi \\ 0 & s\phi/c\theta & c\phi/c\theta \end{pmatrix}. \tag{4}$$

Let $\boldsymbol{\eta} = (\boldsymbol{\eta}_1^T, \boldsymbol{\eta}_2^T)^T$, where $\boldsymbol{\eta}_1 = (x, y, z)^T$ and $\boldsymbol{\eta}_2 = (\phi, \theta, \psi)^T$. $J(\boldsymbol{\eta}_2)$ is the rotation matrix from the body- to the earth-fixed coordinate system. Meanwhile, s, c, and t are the cosine, sine, and tangent functions, respectively. $J_1(\boldsymbol{\eta}_2)$ and $J_2(\boldsymbol{\eta}_2)$ are the linear and angular velocity transform matrices, respectively. In addition, since $J_1(\boldsymbol{\eta}_2)$ is a square and orthogonal matrix, it generally has an inverse matrix and is therefore a singular matrix, but in $J_2(\boldsymbol{\eta}_2)$, there is a term that diverges to infinity when θ is $\pm 90^\circ$. Therefore, $J(\boldsymbol{\eta}_2)$ is not a singular matrix.

3.2. Forces Affecting the Behavior of Towfish

Figure 3 shows the forces affecting the behavior of towfish. For the towfish motion, the towing force $\boldsymbol{f_c} \in R^3$ by the cable and the restoring force $\boldsymbol{f_b} \in R^6$ by the centers of gravity CG and buoyancy CB are applied. In addition, the actuator force $\boldsymbol{f_a} \in R^3$ by the left elevator angle δ_l and right elevator angles δ_r used to control towfish's attitude is generated. Herein, we derive the 6-DOF dynamic motion equation of the towfish using these forces.

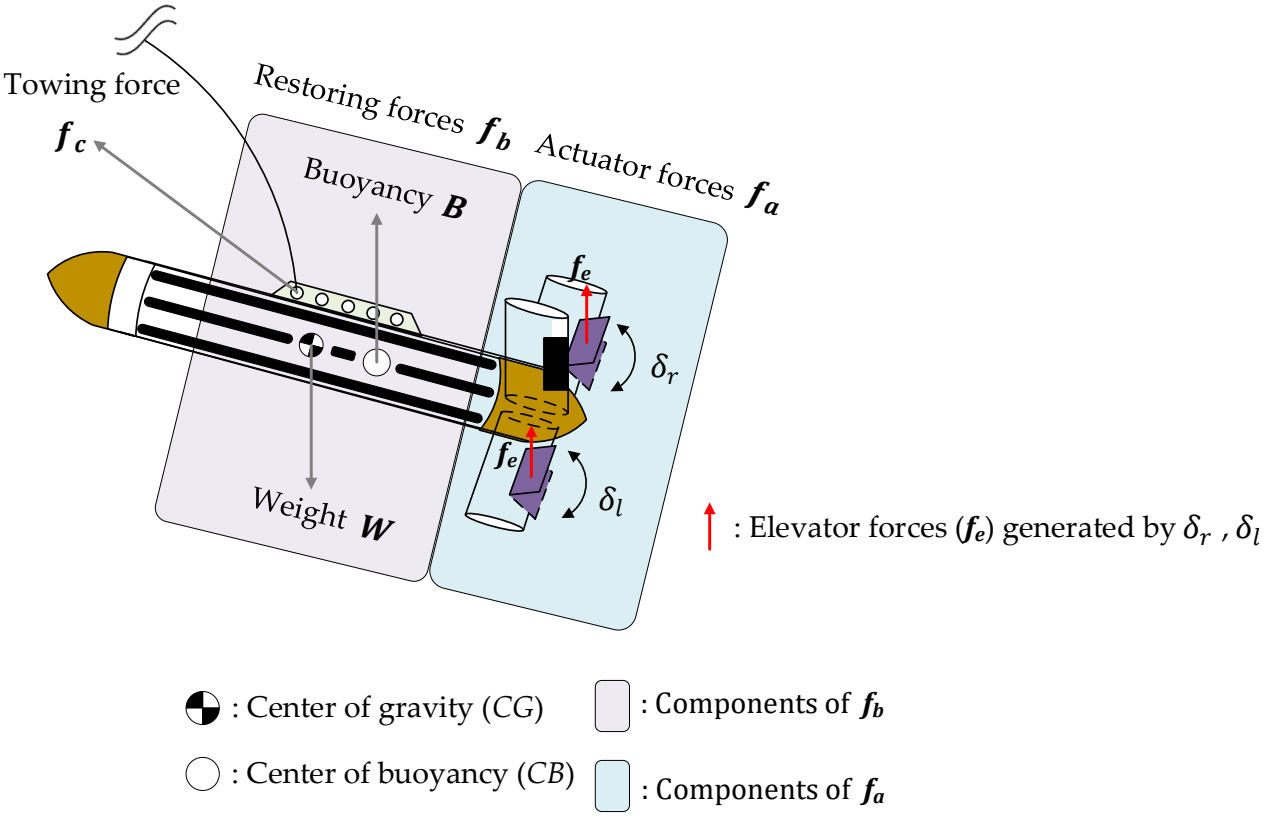


Figure 3. Forces affecting the behavior of towfish.

3.3. Dynamic Equation of Motion for the Towfish

The 6-DOF dynamic equation of motion for the towfish can be written as

$$M\dot{\boldsymbol{\nu}} + C(\boldsymbol{\nu})\boldsymbol{\nu} + D(\boldsymbol{\nu})\boldsymbol{\nu} = \begin{pmatrix} \boldsymbol{f_c} \\ \boldsymbol{r_c} \times \boldsymbol{f_c} \end{pmatrix} + \begin{pmatrix} \boldsymbol{f_a} \\ \boldsymbol{r_a} \times \boldsymbol{f_a} \end{pmatrix} + \boldsymbol{f_b}, \tag{5}$$

where $\boldsymbol{\nu} = (u, v, w, p, q, r)^T \in R^6$ represents the linear and angular velocities of the towfish. $\boldsymbol{r_a} \in R^3$ is the position vector from the CG to the center of elevators, whereas $\boldsymbol{r_c} \in R^3$ is the position vector from the CG to the towing point. M, $C(\boldsymbol{\nu})$, and $D(\boldsymbol{\nu})$ are the inertia matrix, Coriolis and centripetal matrix, and damping term, respectively. $\times$ is the vector outer product.

The inertia matrix M can be expressed as [24]

$$M = [M_{RB} + M_A] \in R^{6\times 6}, \tag{6}$$

$$M_{RB} = \begin{pmatrix} m & 0 & 0 & 0 & mz_g & -my_g \\ 0 & m & 0 & -mz_g & 0 & mx_g \\ 0 & 0 & m & my_g & -mx_g & 0 \\ 0 & -mz_g & my_g & I_{xx} & 0 & 0 \\ mz_g & 0 & -mx_g & 0 & I_{yy} & 0 \\ -my_g & mx_g & 0 & 0 & 0 & I_{zz} \end{pmatrix}, \tag{7}$$

$$M_A = -\mathrm{diag}\left(X_{\dot{u}}, Y_{\dot{v}}, Z_{\dot{w}}, K_{\dot{p}}, M_{\dot{q}}, N_{\dot{r}}\right)^T. \tag{8}$$

The inertia matrix M can be expressed as the sum of the rigid-body inertial matrix M_{RB} and added mass matrix M_A. Herein, m is the mass of the towfish, and (x_g, y_g, z_g) is the coordinates of CG. (I_{xx}, I_{yy}, I_{zz}) is the moment of inertia about the body-fixed coordinate system. $\left(X_{\dot{u}}, Y_{\dot{v}}, Z_{\dot{w}}, K_{\dot{p}}, M_{\dot{q}}, N_{\dot{r}}\right)$ represents the hydrodynamic coefficients.

The Coriolis and centripetal matrix $C(\boldsymbol{\nu})$ can be expressed as [25]

$$C(\boldsymbol{\nu}) = C_{RB}(\boldsymbol{\nu}) + C_A(\boldsymbol{\nu}) \in R^{6\times 6}, \tag{9}$$

$$C_{RB} \begin{pmatrix} 0 & 0 & 0 & m(y_g q + z_g r) & -m(x_g q - w) & -m(x_g r + v) \\ 0 & 0 & 0 & -m(y_g p + w) & m(z_g r + x_g p) & -m(y_g r - u) \\ 0 & 0 & 0 & -m(z_g p - v) & -m(z_g q + u) & m(x_g p + y_g q) \\ -m(y_g q + z_g r) & m(y_g p + w) & m(z_g p - v) & 0 & I_{zz} r & -I_{yy} q \\ m(x_g q - w) & -m(z_g r + x_g p) & m(z_g q + u) & -I_{zz} r & 0 & I_{xx} p \\ m(x_g r + v) & m(y_g r - u) & -m(x_g p + y_g q) & I_{yy} q & -I_{xx} p & 0 \end{pmatrix}, \tag{10}$$

$$C_A = \begin{pmatrix} 0 & 0 & 0 & 0 & -Z_{\dot{w}} w & Y_{\dot{v}} v \\ 0 & 0 & 0 & Z_{\dot{w}} w & 0 & X_{\dot{u}} u \\ 0 & 0 & 0 & -Y_{\dot{v}} v & X_{\dot{u}} u & 0 \\ 0 & -Z_{\dot{w}} w & Y_{\dot{v}} v & 0 & -N_{\dot{r}} r & M_{\dot{q}} q \\ Z_{\dot{w}} w & 0 & X_{\dot{u}} u & N_{\dot{r}} r & 0 & -K_{\dot{p}} p \\ -Y_{\dot{v}} v & X_{\dot{u}} u & 0 & -M_{\dot{q}} q & K_{\dot{p}} p & 0 \end{pmatrix}. \tag{11}$$

The Coriolis and centripetal matrix $C(\boldsymbol{\nu})$ comprises the sum of rigid-body Coriolis and centripetal matrix $C_{RB}(\boldsymbol{\nu})$ and hydrodynamic Coriolis and centripetal matrix $C_A(\boldsymbol{\nu})$.

The damping term $D(\boldsymbol{\nu})$ can be expressed as [26]

$$D(\boldsymbol{\nu}) = D + D_n(\boldsymbol{\nu}) \approx D \in R^{6\times 6}, \tag{12}$$

$$D = -\mathrm{diag}\left(X_u, Y_v, Z_w, K_p, M_q, N_r\right)^T. \tag{13}$$

The damping term $D(\boldsymbol{\nu})$ comprises the sum of the linear and nonlinear damping terms. However, as the maximum speed of the towfish used is not high (2 m/s), the nonlinear damping term is ignored and is instead defined as $D(\boldsymbol{\nu}) = D \in R^{6\times6}$.

The restoration of force $\boldsymbol{f_b}$ can be expressed as [27]

$$\boldsymbol{f_b} \in R^6 = \begin{pmatrix} -(W-B)\mathrm{s}\theta \\ (W-B)s\theta\mathrm{s}\phi \\ (W-B)c\theta\mathrm{c}\phi \\ \left(y_g W - y_b B\right)\mathrm{c}\theta\mathrm{c}\phi - \left(z_g W - z_b B\right)c\theta\mathrm{s}\phi \\ -\left(z_g W - z_b B\right)s\theta - \left(x_g W - x_b B\right)c\theta\mathrm{c}\phi \\ \left(x_g W - x_b B\right)c\theta\mathrm{s}\phi + \left(y_g W - y_b B\right)\mathrm{s}\theta \end{pmatrix}, \tag{14}$$

where $(x_b,\ y_b,\ z_b)$ is the coordiantes of the CB.

4. Calculation of the Controllable Region for Attitude Control of the Towfish

The roll, pitch, and yaw motions of the towfish are not generated by a single motion but are all caused by the interaction of complex motions. Therefore, we intend to derive the region of the towing point where the attitude can be controlled by utilizing the 6-DOF dynamic motion equation of the towfish derived as in Section 3. In particular, when the towfish reaches a certain speed, there is almost no change in the heading angle, and the roll motion is naturally restored due to the towfish's weight and the vertical force of the cable. Therefore, it is very important to control the pitch angle in order to improve the image quality of sonar mounted on the towfish. For this reason, this study aimed to determine the towing point region, where the pitch angle control of the towfish. The dynamic forces affecting the behavior of the towfish in the $x-z$ plane during pitch motion are shown in Figure 4.

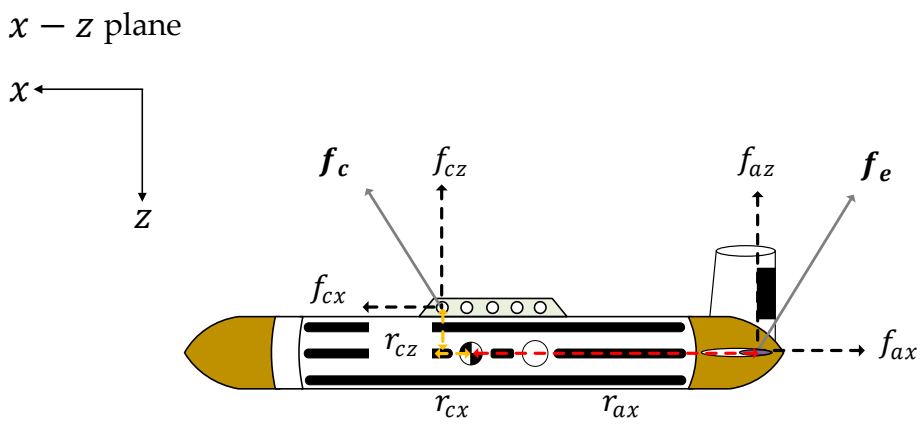


Figure 4. Dynamic forces affecting the behavior of towfish in the $x-z$ plane.

Figure 4 shows the dynamic forces affecting the behavior of towfish in the $x-z$ plane, where $\boldsymbol{f_c} = (f_{cx},\ f_{cz})^T$ and $\boldsymbol{f_e} = (f_{ax},\ f_{az})^T$ are the towing and actuator drag forces, respectively. $\boldsymbol{r_c} = (r_{cx},\ r_{cz})^T$ is the position vector from the CG to the TP, whereas $\boldsymbol{r_e} = (r_{ax}, 0)^T$ is the position vector from the CG to the actuator center. Considerably, the itching moment of the towfish caused by the towed, restoring, and actuator drag forces on the $x-z$ plane can be calculated as follows:

$$M_y = \boldsymbol{r_c} \bigotimes \boldsymbol{f_C} + \boldsymbol{r_e} \bigotimes \boldsymbol{f_e} + f_{b5}, \tag{15}$$

where f_{b5} is the fifth term in Equation (14) and $\otimes$ represents the vector outer product on the plane. The vector outer product on the plane has the relationship $\boldsymbol{a} \otimes \boldsymbol{b} = (E\boldsymbol{a})^T \boldsymbol{b} = (E^T \boldsymbol{a}^T)\boldsymbol{b},\ \boldsymbol{a}, \boldsymbol{b} \in R^2$, where E is the rotation matrix rotated 90° counterclockwise on the plane and is given as follows:

$$E = \begin{pmatrix} 0 & -1 \\ 1 & 0 \end{pmatrix}. \tag{16}$$

Because the pitching moment direction and force of the towfish change per the towing point and positions of the CG and CB, they must be analyzed for each case. Herein, the three cases given in Figure 5 were selected and analyzed.

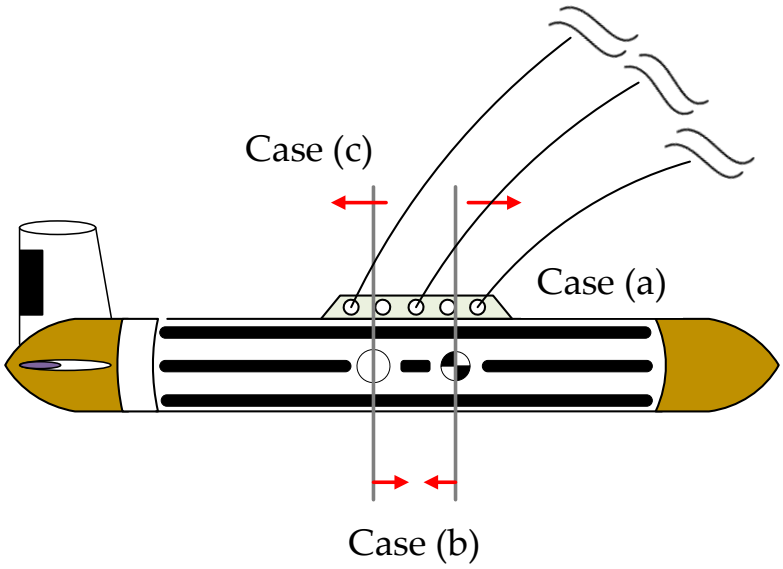


Figure 5. Three cases for interpreting the controllable region.

In general, while operating the towfish, the CG is positioned in front of CB to alleviate the vertical force caused by the cable, thereby ensuring stability. In contrast, if the CB is positioned in front of the CG, ensuring the stability of the towfish is difficult. Thus, this study evaluated a case where the CG was in front of the CB.

As shown in Figure 5, the case where the CG is ahead of the CB is selected; however, selecting an appropriate towing point is crucial. The towing point can be physically divided into three cases: when the towing point is (case (a)) ahead of the CG, (case (b)) between the CG and the CB, and (case (c)) behind the CB.

4.1. Controllable Region of the Towing Point That Can Control the Pitch Control

In cases (a)–(c), because the CG is in front of the CB, a restoring force occurs naturally. Therefore, the influence of the restoring force cannot be ignored. The restoring force term f_{b5} is $-(z_g W - z_b B)s\theta - (x_g W - x_b B)c\theta c\phi$ and can be simplified to $-x_g W$ when the towfish is stabilized $(\theta,\ \phi \approx 0^\circ)$ and the CB is located at the origin. Therefore, the maximum and minimum towing points can be obtained as follows:

$$\begin{aligned} r_{cx\ \max}^{+} &= \frac{r_{cz} f_{cx} + r_{ax} f_{az\ \max}^{-} + x_g W}{f_{cz}}, \\ r_{cx\ \max}^{-} &= -\left(\frac{-r_{cz} f_{cx} + r_{ax} f_{az\ \max}^{+} + x_g W}{f_{cz}} \right). \end{aligned} \tag{17}$$

$f_{az\ \max}^{+}$ is the maximum drage force occuring at the maximum angle in the positive direction of the elevator and $f_{az\ \max}^{-}$ is the maximum drage force occuring at the maximum angle in the negative direction of the elevator. Herein, the positive direction is the opposite direction of the z-axis in the body-fixed coordinate system of the towfish, whereas the

negative direction is the direction of the z-axis. The maximum towing point at the instant when the pitching moment becomes positive is $r^{+}_{cx\ \max}$ and the maximum towing point at the instant when the pitching moment becomes negative is $r^{-}_{cx\ \max}$. Therefore, when the towing points of the towfish are $r^{+}_{cx\ \max}$ and $r^{-}_{cx\ \max}$, it can be divided into regions where attitude control is possible and impossible, respectively. This means that if the towing point exceeds $r^{+}_{cx\ max}$ and $r^{-}_{cx\ max}$, the pitch control of the towfish will be impossible.

4.2. Simulation

A simulation was conducted to demonstrate the controllable region of the towing point. The drag forces occurring by the elevators were as follows:

$$\begin{gathered} f_{ax} = C_A C_D + C_A C_D, \\ f_{az} = C_A C_L + C_A C_L, \\ C_L, C_D = \text{function of } \alpha,\ C_A = 0.5 \rho s_A u^2, \end{gathered} \tag{18}$$

where ρ, s_A, and u are the density of water, area of the single elevator and forward speed of the towfish, respectively. α is the angle of attack. C_D and C_L are the drag and lift coefficients, respectively. NACA gives values of C_D and C_L according to the shape of the wing. The wing shape is NACA 0018, and the C_D and C_L values for this shape are as shown in Figure 6. The drag coefficient is determined by the speed of the towfish and the elevator area, and the lift and drag coefficients use the values provided according to the elevator angle with reference to Figure 6. Hence, among the wing shapes provided by NACA, NACA 0018 has the advantage of being symmetrical from top to bottom, and the elevator area in the positive and negative directions is the same, making it useful for elevator angle control. For this reason, NACA 0018 was selected in this study.

Because the elevator angle indicates the angle of attack [28], f_{ax} and f_{az} are written as a function of the elevator angle. δ_r is the angle of the right elevator and δ_l is the angle of the left elevator. The mathematical model of the towfish used in the simulation based on Equations (1) and (18) is as follows:

$$\begin{aligned} & M\dot{\boldsymbol{\nu}} + C(\boldsymbol{\nu})\boldsymbol{\nu} + D(\boldsymbol{\nu})\boldsymbol{\nu} - \boldsymbol{f_b} - \begin{pmatrix} f_c \\ r_c \times f_c \end{pmatrix} \\ &= \begin{pmatrix} -(C_D/\delta_r) C_A & -(C_D/\delta_r) C_A \\ 0 & 0 \\ (C_L/\delta_r) C_A & (C_L/\delta_r) C_A \\ 0 & 0 \\ (C_L/\delta_r) C_A r_{ax} & (C_L/\delta_r) C_A r_{ax} \\ 0 & 0 \end{pmatrix} \begin{pmatrix} \delta_r \\ \delta_l \end{pmatrix}. \end{aligned} \tag{19}$$

Table 2 shows the values of hydrodynamic derivatives for the towfish used in the simulation. The rotational moments of inertia I_{xx}, I_{yy} and I_{zz} were calculated using cylindrical features, whereas $X_{\dot{u}}$, $Y_{\dot{v}}$, $Z_{\dot{w}}$, $K_{\dot{p}}$, $M_{\dot{q}}$ and $N_{\dot{r}}$ were calculated with reference to the towfish's specifications. The remaining hydrodynamic derivatives X_u, Y_v, Z_w, K_p, M_q and N_r were selected through simulation. Meanwhile, since the towfish is controlled by the left and right elevator angles, which are the outputs of the controller, Equation (18) was slightly modified to extract only the δ_r and δ_l terms as in Equation (19) and reflected in the simulation.

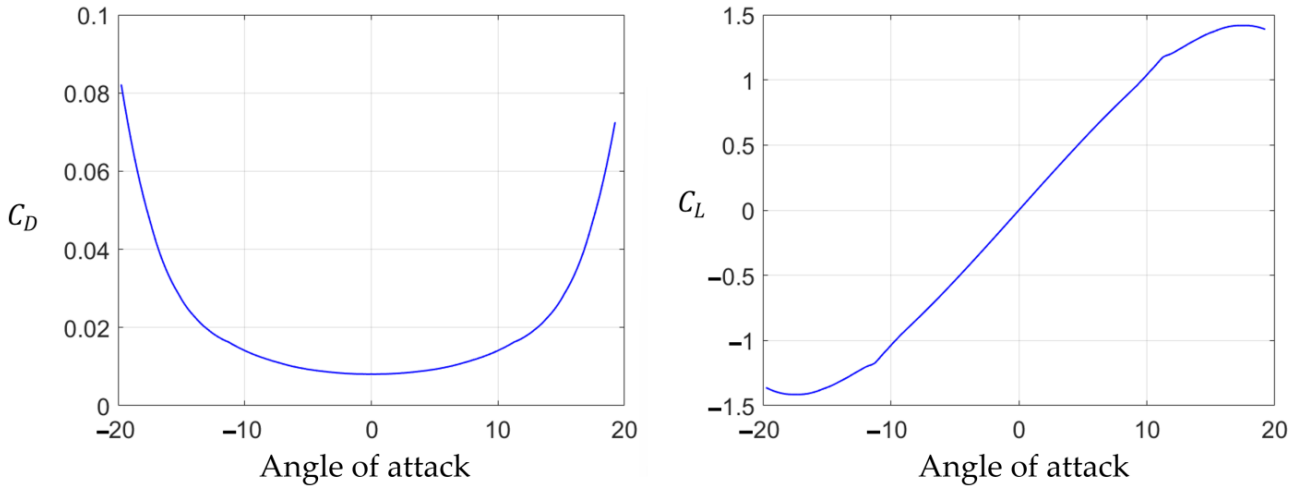


Figure 6. C_D and C_L values when the wing shape is NACA0018.

Table 2. Values of hydrodynamic derivatives for the towfish.

Hydrodynamic Derivatives	Values	Hydrodynamic Derivatives	Values
m	300 kg	$M_{\dot{q}}$	−144.4516 kg
I_{xx}	6 kgm^2	$N_{\dot{r}}$	−144.4516 kg
I_{yy}	309.25 kgm^2	X_u	−20 kg/s
I_{zz}	309.25 kgm^2	Y_v	−200 kg/s
$X_{\dot{u}}$	−12.837 kg	Z_w	−200 kg/s
$Y_{\dot{v}}$	−276.2693 kg	K_p	−30 kgm^2/s
$Z_{\dot{w}}$	−276.2693 kg	M_q	−300 kgm^2/s
$K_{\dot{p}}$	0 kg	N_r	−300 kgm^2/s

In this study, the parameter values considered to obtain the controllable region of the towing point are the towing speed and the CG. Therefore, the controllable region of the towing point is calculated by changing the towing speed and the CG. The coordinates of the CG of the towfish are 0 m along the y and z axes and change only along the x-axis, so the coordinates for the x-axis were changed. The simulation was conducted while changing the towing speed and position of x_g from 1 to 2 m/s and 0 to 0.5 m, respectively, to calculate the controllable region of the towing point. Presumably, the force is balanced by generating a towing force f_{cz} of −2450 N in the direction opposite to the underwater weight $(W - B)$ of the towfish. In the specifications of the towfish, r_{cz} is 0.2 m; when x_g is at the center of towifsh, r_{ax} is 1.7 m. Figure 7 demonstrates the results of the calculation of the region of the towing point where the attitude of the towfish can be controlled using the dynamic equation of the towfish.

Figure 7 shows the controllable region of the r_{cx} when the towing speed changes from 1 to 2 m/s and x_g changes from 0 to 0.5 m. The region surrounded by the black solid line is the $r^{+}_{cx\ \max}$ region where the elevator drag force is maximum in the negative direction. Meanwhile, the region surrounded by the red solid line is the $r^{-}_{cx\ \max}$ region where the elevator drag force is maximum in the positive direction. As shown in the simulation results, as the towing speed of the towfish increases, the range of the controllable towing point widens; this is because the drag force occurring by the elevator increases as the towing speed increases.

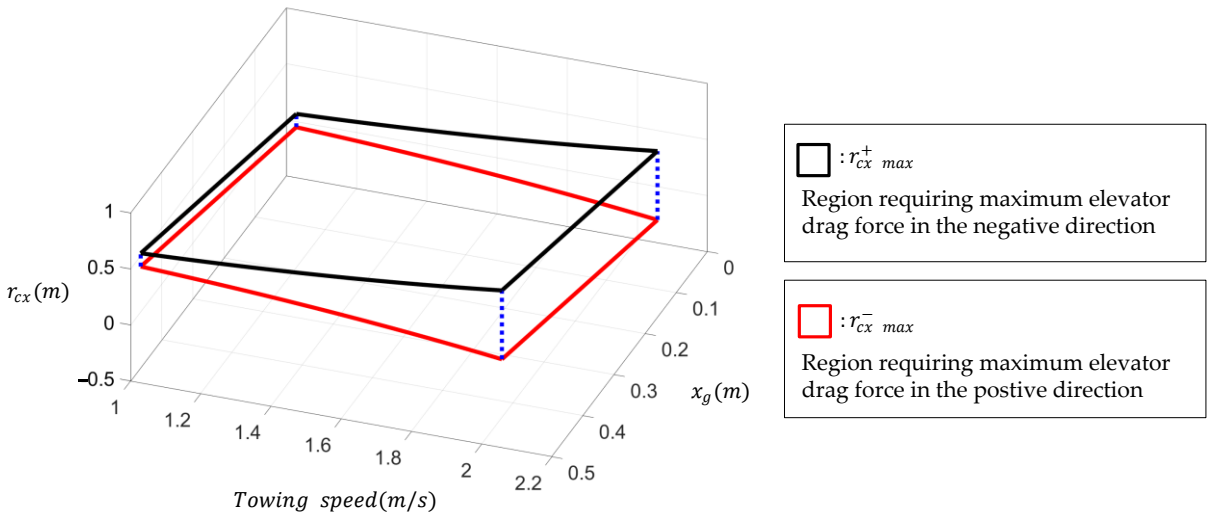


Figure 7. Controllable region of the r_{cx} when the towing speed and x_g change.

Therefore, to control the attitude of the towfish will be difficult in regions surrounded by the red and black lines because these are the regions where the maximum elevator drag force occurs. Therefore, to reliably control the attitude of the towfish, the towing point should be selected between the two regions.

To examine the presented cases in detail, the regions for cases (a)–(c) are presented (Figure 8).

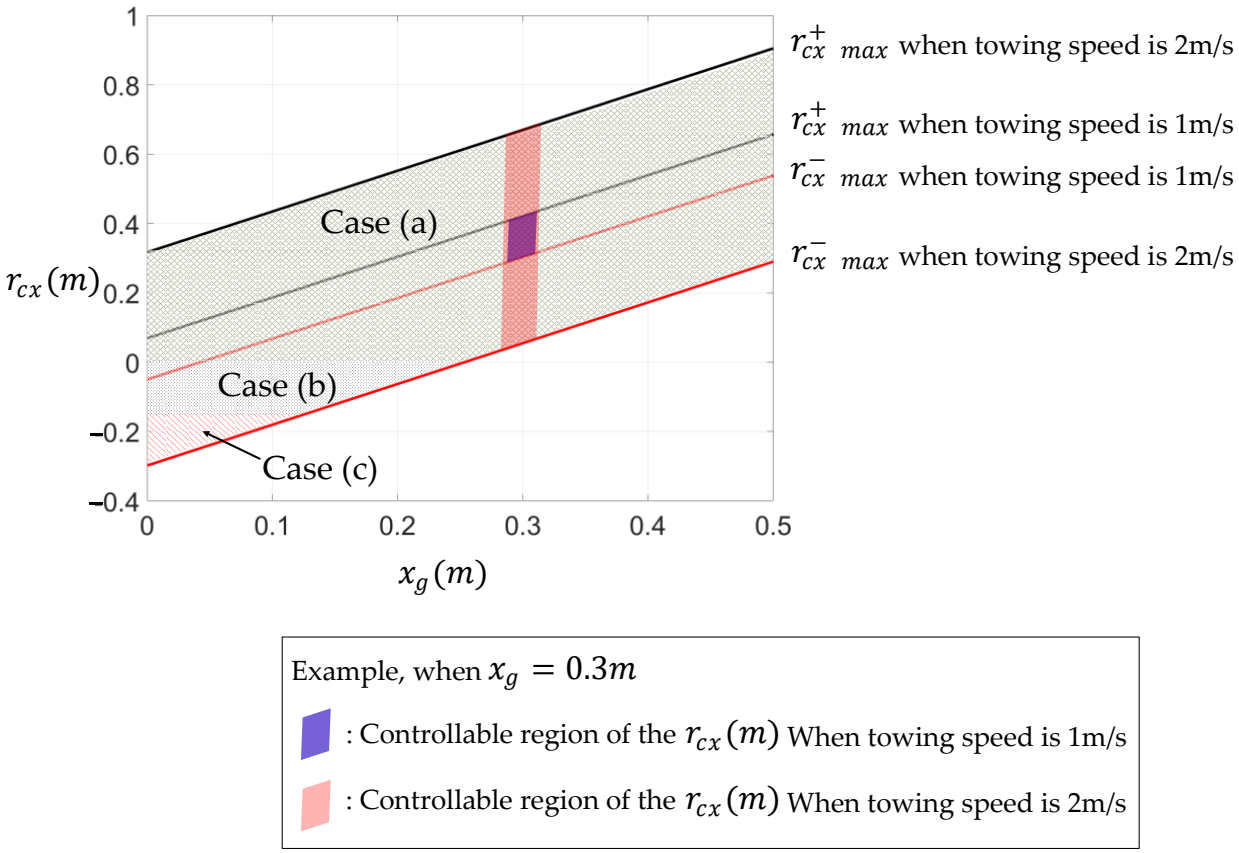


Figure 8. Controllable region of the towing point about cases (a)–(c).

Figure 8 denotes the controllable region of the towing point of the towfish for cases (a)–(c). For interpretation, the controllable region is indicated in the r_{cx} and x_g axes.

In case (a), where the towing point is positioned ahead of the *CG*, the controllable region of the towing point is widespread. At a towing speed of 1 m/s, the controllable region is somewhat narrow, but as the towing speed increases, it widens substantially. This is because the vertical force by the cable naturally restores the pitch angle of the towfish to the horizontal. Meanwhile, in case (c), where the towing point is behind the *CB*, the controllable region is quite narrow. In this case, when the towing speeds are very low, attitude control is challenging; even at sufficient towing speeds, securing the safety of the towfish is difficult. This is because the vertical force by the cable rather acts to increase the pitch angle of the towfish. In case (b), when the towing point is between the *CG* and the *CB*, the controllable region of the towing point is slightly wider than that in case (c) but much narrower than that in case (a).

The blue parallelogram represents the controllable region of the r_{cx} when the x_g and towing speed are 0.3 m and 1 m/s, respectively. Additionally, the red parallelogram represents the controllable region of the r_{cx} when the x_g and towing speed are 0.3 m and 2 m/s, respectively. Apparently, as the towing speed increases, the controllable region of the towing point expands. Consequently, selecting the towing point forward rather than the x_g is advantageous for attitude control when operating the towfish.

5. Water Tank Test

To verify the controllable region of the proposed towing point, a water tank test was conducted. The *CG* of the towfish was naturally fixed while designing so it could not be changed during testing. Therefore, to secure the stability of the towfish, the water tank test was conducted by changing the flow rate of the tank. In the proposed controllable region, the points selected in the water tank test and the x_g position of the towfish are shown in Figure 9.

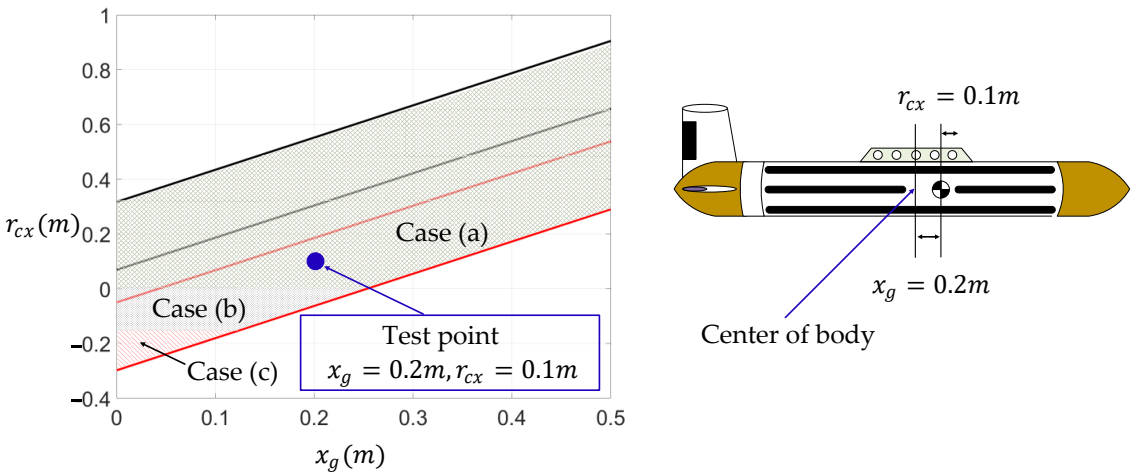


Figure 9. Test points selected for the water tank test and the positions of the *CG* and r_{cx}.

Figure 9 shows the test points selected for the water tank test and the positions of the *CG* and towing point of the towfish. The x_g of the towfish was designed at approximately 0.2 m in front of the center of the body, whereas the towing point was at 0.1 m in front of the x_g.

The water tank test aimed to maintain the pitch angle of the towfish to 0°. The pitch controller is shown in Equation (20).

$$\delta_r, \delta_l = K_p\left(\theta_{ref} - \theta\right) - K_d q + K_i \int_0^t (\theta_{\text{ref}} - \theta), \tag{20}$$

where K_p, K_i, and K_d are the control gains of the proportional–integral–derivative (PID) controller, which are proportional, integral, and derivative gains for the elevator angle, respectively. The control gain values used in the water tank test were $K_p = 3$, $K_i = 0.01$, and $K_d = 5$. θ and θ_{ref} were the current pitch angle and the target pitch angle (reference input) of the towfish, respectively. The pitch motion can be controlled by following the elevator's synchronous angle $\delta_S = (\delta_r + \delta_l)/2$. Moreover, to prevent rapid changes in the pitch angle and ensure the stability of the towfish, the maximum angle of the left and right elevators of the towfish was limited to $\pm 20^\circ$.

In Section 4, the towing point region where the attitude of the towfish can be controlled was calculated by changing the towing speeds from 1 to 2 m/s, and the flow rate of the water tank was selected differently to confirm the cases where attitude control is possible and not possible at the test point, as presented in Figure 9. In this study, 1 knot, where attitude control was not possible, and 3 and 4 knots, where attitude control was possible, were selected, and the water tank test was conducted.

Hence, in this study, the *CG* was located on the center line of the towfish, so the study on roll motion was ignored. However, if the *CG* is not located on the center line of the towfish, the roll phenomenon occurs. Additionally, if roll motion occurs due to unstable current and waves, it needs to be controlled. The roll motion of the towfish can be achieved by controlling the asynchronous elevator angles $\delta_{AS} = (\delta_r - \delta_l)$. Figure 10 shows the sites where an actual water tank test was conducted.

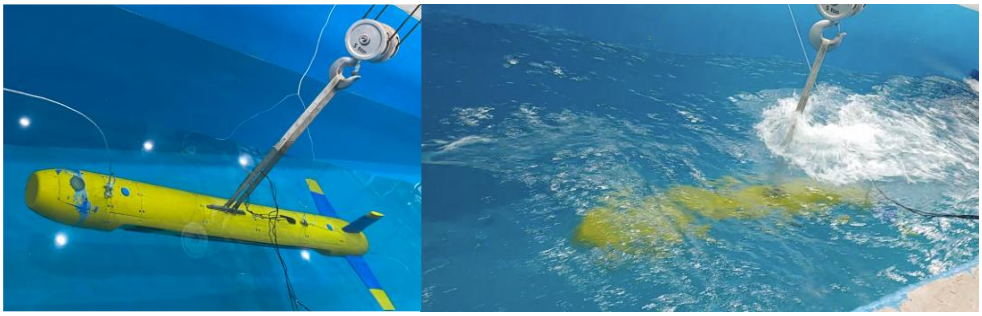


Figure 10. Photo of the actual water tank test site.

5.1. Water Tank Test Configuration Diagram

Figure 11 shows the configuration of the water tank test. The towfish is towed on the working carriage and waits until the flow rate of the water tank that meets the test conditions is generated. Then, when the flow rate of the water tank is satisfied, the pitch angle of the towfish is controlled through the attitude controller, and then information on the attitude and elevator angle is acquired from the self-software using LAN communication.

The test was conducted in a current-generating water tank at the Marine Robot Center of the Korea Institute of Industrial Technology. The spatial velocity distribution of the water tank was measured at a total of 9 points, and at 24 Hz (1.58 m/s) of the impeller, the accuracy was 1.5743 m/s at the maximum, 1.5612 m/s at the minimum, and 1.5666 m/s on average. Therefore, the water tank used in this study can be considered to have a constant flow rate.

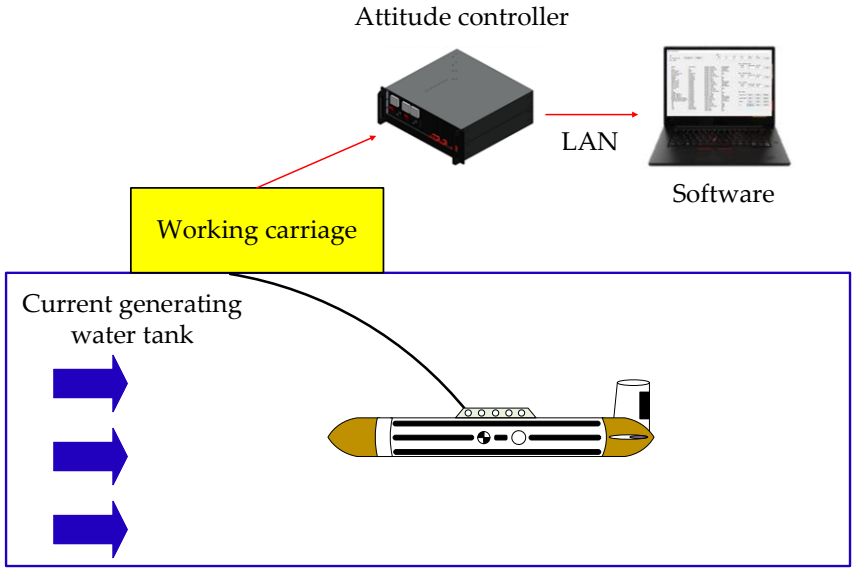


Figure 11. Water tank test configuration diagram.

5.2. Water Tank Test at 1 Knot

Figure 12 shows the results of the attitude control of the towfish when the flow rate of the water tank is 1 knot. Referring to Figures 8 and 9, with the given flow rate, the test point did not exist within the region where the attitude of the towfish could be controlled. Therefore, to satisfy the pitch angle of 0°, δ_S was continuously applied in a positive direction to the maximum angle of 20°. However, the elevator drag force was insufficient to achieve the pitch angle of 0°, which remained at approximately 4°. Moreover, the roll angle was not stabilized at 0° because the vertical force by the cable was insufficiently applied because of the low flow rate of the water tank. Therefore, to control the attitude of the towfish, a sufficient flow rate to generate elevator drag force is required.

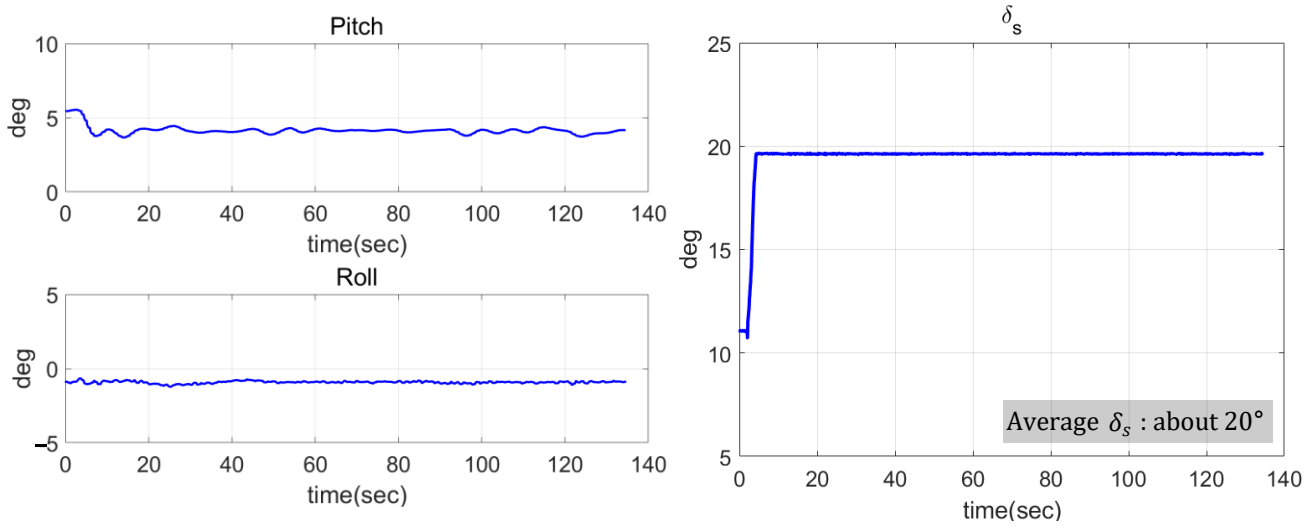


Figure 12. Pitch, roll, and δ_S at 1 knot.

If the towing point is selected in the region where the attitude of the towfish cannot be controlled, the pitch angle cannot be controlled even if left and right elevator angles are applied as much as possible, as in the test results at 1 knot.

5.3. Water Tank Test at 3 Knots

Figure 13 shows the test results of the attitude control of the towfish when the flow rate of the water tank is 3 knots. Pitch control was performed from approximately 20 to 150 s. At this flow rate, the attitude of the towfish could be controlled. Therefore, the target pitch angle of 0° of the towfish could be achieved. To control the pitch angle of the towfish, δ_S occurred around an average of 14°. The elevator angle was not negative because the pitch angle of the towfish naturally rotated in a positive direction owing to the towing force of the cable.

The roll angle could also be reliably maintained at 0° because the vertical force generated by the cable was sufficient and naturally stabilized because of the weight.

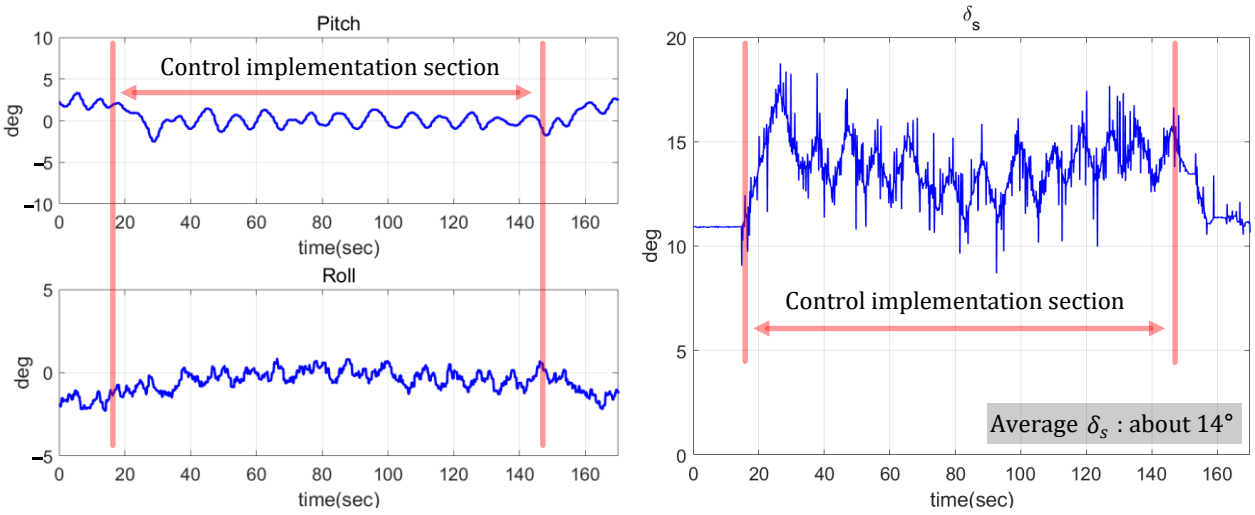


Figure 13. Pitch, roll, and δ_S at 3 knots.

5.4. Water Tank Test at 4 Knot

Figure 14 shows the test results of the towfish when the flow rate of the water tank is 4 knots. This flow rate was also within the controllable region, similar to when the flow rate of the water tank was 3 knots. At this flow rate, the elevator drag force was greater than that at 3 knots. Therefore, the target pitch angle of 0° of the towfish could be achieved with a smaller control amount (δ_S) than that at 3 knots. Apparently, δ_S for controlling the pitch was generated around 10°. Moreover, the roll angle of the towfish was naturally stabilized because the flow rate of the water tank was sufficiently affected.

The water tank test is conducted at 1, 3, and 4 knots, but if the flow rate of the water tank is greater than 4 knots, the drag force applied by the elevators increases accordingly, so the pitch angle of the towfish can be controlled with a smaller δ_S.

This study confirmed that there were regions where the attitude of the towfish could and could not be controlled. In addition, through an additional water tank test, we proved that attitude control was possible and impossible in the controllable and uncontrollable regions, respectively. These findings can be used as indicators for appropriately selecting the towing points of towfish.

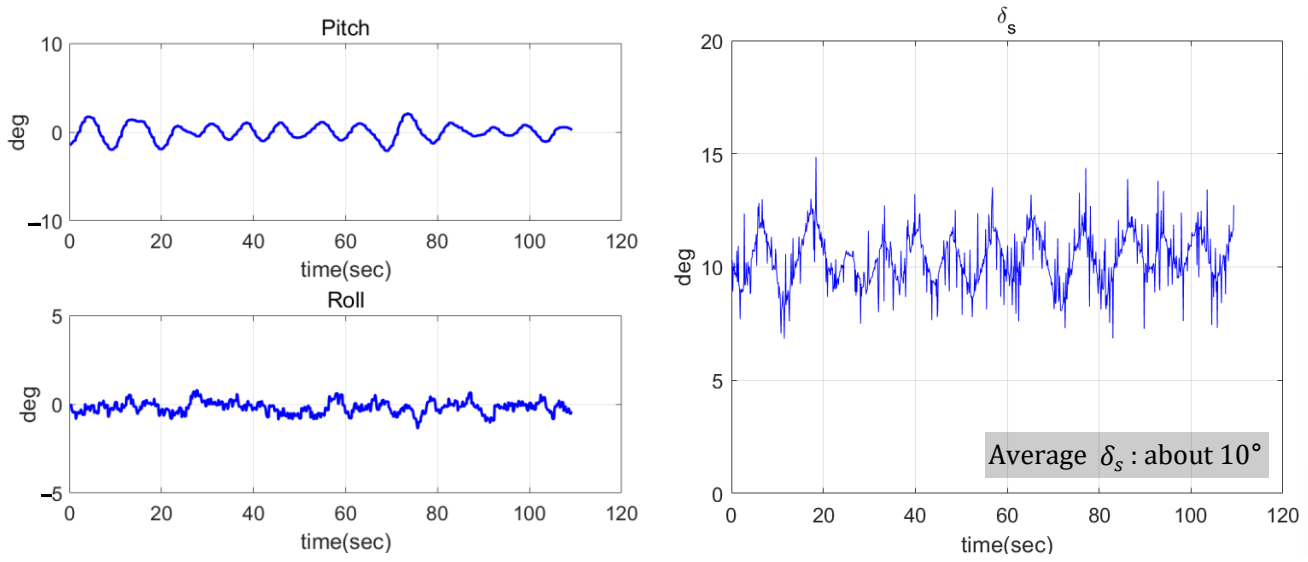


Figure 14. Pitch, roll, and δ_S at 4 knots.

6. Conclusions

We discussed a method for calculating controllable regions to control the attitude of towfish using left and right elevators attached to the horizontal tail wings to improve the sonar image quality.

The towing point, *CG*, elevator drag force, and towing speed were analyzed in a complex manner. Thus, a 6-DOF equation of motion was generated, in which the towing force of the cable and the elevator drag force were added to the body of the towfish. Generally, the *CG* of the towfish is located in front of the *CB* to compensate for the vertical force caused by the cable and secure stability. Therefore, three cases were analyzed in which the *CG* was located in front of the *CB* the towing points were in front of the *CG*, between the *CG* and the *CB*, and behind the *CB*. Based on the generated 6-DOF equation of motion, a controllable region for controlling the attitude of the towfish according to changes in the towing point, *CG*, and towing speed for three cases was presented.

Notably, the range of the controllable region that can control the attitude of the towfish was widespread when the towing point was ahead of the *CG*. In contrast, when the towing point was behind the *CB*, the controllable region was narrow. In all three cases, the elevator drag force that can control the towfish increased as the towing speed increased, making the region that can control the attitude wider. However, when the towing point was behind the *CB*, a towing speed that was fast enough to damage the stability of the towfish was required. Therefore, selecting the case where the towing point is ahead of the *CG* would be advantageous, ensuring the stability of the towfish and allowing various controllable regions.

To verify that the recommended controllable region was correctly selected, a water tank test was conducted. The result of the test at 1 knot, which is out of the region where the attitude of the towfish can be controlled, confirmed that the attitude of the towfish cannot be controlled, and the tests at 3 and 4 knots, which are within the region of the towfish can be controlled, confirmed that the attitude of the towfish can be properly controlled. In the test at 1 knot, since the flow rate of the water is not large, the stability of the towfish is not greatly reduced even if attitude control is not performed. However, if the pitch control is not performed when the flow rate of the water is high, there will be limitations in securing the stability of the towfish. Therefore, it is very important to select the towing point of the towfish appropriately.

In this study, the target towfish is focused on controlling the pitch angle because the *CG* is on the centerline of the towfish, and the analysis of the roll was not conducted. Although the roll motion tends to stabilize from a certain speed, there may be cases where the control of roll is necessary during the test and operation. Therefore, the task remains to derive the region of the towing point that can control the attitude of the towfish, including the roll motion as well as pitch motion.

Author Contributions: Conceptualization, M.-K.K. and J.L.; methodology, M.-K.K.; software, M.-K.K.; validation, J.L. and M.-K.K.; formal analysis, M.-K.K.; investigation, J.L.; resources, J.L.; data curation, M.-K.K.; writing—original draft preparation, J.L.; writing—review and editing, M.-K.K.; visualization, J.L.; supervision, M.-K.K.; project administration, M.-K.K.; funding acquisition, M.-K.K. All authors have read and agreed to the published version of the manuscript.

Funding: This work was supported by Korea Institute of Marine Science & Technology Promotion (KIMST) funded by the Ministry of Oceans and Fisheries (RS-2023-00256122).

Data Availability Statement: The raw data supporting the conclusions of this article will be made available by the authors on request.

Conflicts of Interest: The authors declare no conflicts of interest.

Abbreviations

The following abbreviations are used in this manuscript:

sonar	Sound navigation ranging
InSAS	Interferometric synthetic aperture sonar
6-DOF	Six-degree-of-freedom
CFD	Computational fluid dynamics
USBL	Ultra-short baseline
IMU	Inertial measurement unit
NACA	National Advisory Committee for Aeronautics

References

1. Pang, S.K.; Li, Y.H.; Yi, H. Joint formation control with obstacle avoidance of towfish and multiple autonomous underwater vehicles based on graph theory and the null-space-based method. *Sensors* **2019**, *19*, 2591. [CrossRef] [PubMed]
2. Go, G.; Ahn, H.T. Hydrodynamic derivative determination based on CFD and motion simulation for a tow-fish. *Appl. Ocean Res.* **2018**, *82*, 191–209. [CrossRef]
3. Yang, S.; Zhu, X.; Ren, H. Dynamic analysis of a deep-towed seismic system based on a flexible multi-body dynamics frame. *Ocean Eng.* **2023**, *279*, 114587. [CrossRef]
4. Campagnaro, F.; Steinmetz, F.; Renner, B.C. Survey on low-cost underwater sensor networks: From niche applications to everyday use. *J. Mar. Sci. Eng.* **2023**, *11*, 125. [CrossRef]
5. Zhang, C.; Xiao, F. Overview of data acquisition technology in underwater acoustic detection. *Procedia Comput. Sci.* **2021**, *188*, 130–136. [CrossRef]
6. Neupane, D.; Seok, J. A review on deep learning-based approaches for automatic sonar target recognition. *Electronics* **2020**, *9*, 1972. [CrossRef]
7. Lee, J.; Oh, Y.; Park, S.; Kim, H. Development of towed synthetic aperture sonar system. *Korea Soc. Nav. Sci. Technol.* **2019**, *2*, 28–31. [CrossRef]
8. Hansen, R.E.; Saebo, T.O.; Gade, K.; Chapman, S. Signal processing for AUV based interferometric synthetic aperture sonar. In Proceedings of the OCEANS 2003, San Diego, CA, USA, 22–26 September 2003.
9. Teixeira, F.C.; Aguiar, A.P.; Pascoal, A. Nonlinear adaptive control of an underwater towed vehicle. *Ocean Eng.* **2010**, *37*, 1193–1220. [CrossRef]
10. Cammarata, A.; Sinatra, R. Parametric study for the steady-state equilibrium of a towfish. *J. Intell. Robot. Syst.* **2015**, *81*, 231–240. [CrossRef]
11. Droppers, J.C.; Fisher, W.; Predmyrskyy, A. Tow-body control system modeling and tuning on a real-world vehicle. In Proceedings of the OCEANS 2023, Limerick, Ireland, 5–8 June 2023.

12. Muscat, M.; Cammarate, A.; Maddio, P.D.; Sinatra, S. Design and development of a towfish to monitoe marine pollution. *Euro-Mediterr. J. Environ. Integr.* **2018**, *3*, 11. [CrossRef]
13. Park, J.; Kim, N. Dynamics modeling of a semi-submersible autonomous underwater vehicle with a towfish towed by a cable. *Int. J. Nav. Archit. Ocean Eng.* **2015**, *7*, 409–425. [CrossRef]
14. Artur, G.; Andrzej, F.; Mariusz, W. Ecperience with the use of a rigidly-mounted side-scan sonar in a harbor basin bottom investigation. *Ocean Eng.* **2015**, *109*, 439–443. [CrossRef]
15. Lambert, C.; Nahon, M.; Buckham, B.; Seto, M. Dynamics and control of towed underwater vehicle system, part II: Model validation and turn maneuver optimization. *Ocean Eng.* **2003**, *30*, 471–485. [CrossRef]
16. Buckham, B.; Nahon, M.; Seto, M.; Zhao, X.; Lambert, C. Dynamics and control of towed underwater vehicle system, part I: Model development. *Ocean Eng.* **2003**, *30*, 453–470. [CrossRef]
17. Seto, M.T.; Watt, G.D.; Hopkin, D. A fully interactive dynamic simulation of a semi-submersible towing a large towfish. In Proceedings of the OCEANS 99, Seattle, WA, USA, 13–16 September 1999.
18. Koterayama, W.; Kyozukw, Y.; Nakamura, M.; Ohkusu, M.; Kashiwagi, M. The motion of a depth controllable towed vehicle. *Offshore Mech. Artic Eng.* **1998**, *1*, 423–430.
19. Kim, J. Adaptive Coverage Path planning for underwater sonar scans in environments with changing current. *J. Mar. Sci. Eng.* **2025**, *13*, 118. [CrossRef]
20. Yang, S.; Ren, H.; Zhu, X. Dynamic modeling of cable deployment/retrieval based on ALE-ANCF and adaptive step-size integrator. *Ocean Eng.* **2014**, *309*, 2. [CrossRef]
21. Go, G.; Lee, E.; Ahn, H.T.; Chun, S.Y. 6DOF simulation and determination of hydrodynamic derivatives of underwater tow-fish using CFD. *J. Soc. Nav. Archit. Korea* **2016**, *53*, 315–328. [CrossRef]
22. Kim, M.K.; Park, D.J.; Kim, J.H.; Choi, J.K. Feasuble positions of towing point and center of gravity for towfish attitude control. *J. Ocean Eng. Technol.* **2020**, *34*, 334–341. [CrossRef]
23. Kim, M.K.; Park, D.J.; Oh, Y.S.; Kim, J.H.; Choi, J.K. Towfish Attitude Control: A Consideration of Towing Point, Center of Gravity, and Towing Speed. *J. Mar. Sci. Eng.* **2021**, *6*, 641. [CrossRef]
24. Holger, K. Track Control of a Towed Underwater Sensor Carrier. *IFAC Proceeding Vol.* **2000**, *33*, 89–94.
25. Fossen, T.I. *Handbook of Marine Craft Hydrodynamics and Motion Control*; John Willy & Sons Ltd.: Sussex, UK, 2011.
26. Fossen, T.I. *Marine Control Systems*; Marine Cybernetics: Trondheim, Norway, 2001.
27. Fossen, T.I. *Guidance and Control of Ocean Vehicles*; John Willy & Sons Ltd.: Sussex, UK, 1994.
28. Park, C.; Shin, M.; Choi, J.; Hwang, H.; Shin, Y.; Kim, Y. An experimental study on effect of angle of attack on elevator control force for underwater vehicle with separate fixed fins. *Ocean Eng. Technol.* **2016**, *30*, 243–252. [CrossRef]

Disclaimer/Publisher's Note: The statements, opinions and data contained in all publications are solely those of the individual author(s) and contributor(s) and not of MDPI and/or the editor(s). MDPI and/or the editor(s) disclaim responsibility for any injury to people or property resulting from any ideas, methods, instructions or products referred to in the content.